

Implementation of Modified Cam-Clay Model using Closest Point Projection Method

Chao Xu¹

¹College of Civil Engineering and Architecture, Zhejiang University, Hangzhou, Zhejiang, China

Article Info

Volume 83

Page Number: 4507 - 4515

Publication Issue:

July-August 2020

Abstract

The modified Cam-Clay model is a widely used constitutive model of soft clay in geotechnical engineering. It can describe the behaviors of soft clay well. Therefore, this model is used in many numerical analyses to get better results. However, many derivations of the integration of the elastoplastic stress are in the $p'-q$ plane which geotechnical engineers are familiar with. In this paper, the closest point projection method is used for integrating the stress of the modified Cam-Clay model. In addition, the plasticity of the model and the equations used in the closest point projection method are derived in detail under the Cartesian coordinate space. Subsequently, a UMAT subroutine of ABAQUS is developed using FORTRAN. Finally, a triaxial test under drainage consolidation with three consolidation states is calculated using the analytical equations, the ABAQUS built-in model, and the UMAT model respectively for verifications. Results show that the proposed method is feasible and stable, and all three types of results using different methods are the same, it is proved that the UMAT model is accurate enough for analyses.

Keywords: modified Cam-Clay Model, closest point projection method, finite element method, soft clay, ABAQUS.

Article History

Article Received: 25 April 2020

Revised: 29 May 2020

Accepted: 20 June 2020

Publication: 10 August 2020

I. Introduction

The soft clay exists in the real world extensively, and it has many particular features that are absent in many types of soils. Hence, many soil models cannot be used to represent the behaviors of the soft clay, and corresponding calculation methods cannot solve the settlement of the soft soil. In the past decades, many engineers and scholars are dedicated to improving the calculation of soft clay.

During the period from 1958 to 1963, Roscoe [1,2] and his colleagues proposed the Cam-Clay model based on a large number of triaxial tests of saturated clay at Cambridge University. The model adopts the cap yield surface and the associated flow criterion and takes the plastic volume strain as the hardening parameter. In addition, this model theoretically explains the elastoplastic deformation characteristics of soft clay. It greatly accelerates the

development of the constitutive model of soft soil. Many finite element software in geotechnical engineering have used this model. However, experiments have shown that when the shear stress is small, the calculated value of the shear strain given by the Cam-Clay model is larger. To tackle the problem, Burland [3] used a new incremental plastic energy formula to modify the model and get the modified Cam-Clay model.

After that, the modified Cam-Clay model is broadly used in engineering projects, such as the tunnel construction built on soft ground [4], the pile installation [5], and the analysis of instability [6]. Especially, analyses of the deep excavations [7-10] and projects built on clay [9,11,12] use the model widely. However, the analytical solution of the modified Cam-Clay model is too hard to be applied to many situations. Therefore, its numerical

solution, for example, the finite element solution, are also researched extensively. From the aspects of implementations [13-20] to the extensions of the original model [13,21,22], the modified Cam-Clay model is improved heavily in the past. Nevertheless, many implementations are based on the triaxial stress space [14,18-20,23,24], the considerations of stress statuses in the Cartesian coordinate system are lack. This paper gives the derivations of integration using the closest point projection method and implements the finite element subroutines of the modified Cam-Clay model in ABAQUS. Finally, examples are conducted for verifying the feasibility, stability, and accuracy.

II. METHODOLOGY

Yield function of the model

Roscoe firstly proposed the yield equation of the Cam-Clay model as shown in Equation(1), it is the most important formula of the Cam-Clay model.

$$f = \frac{q}{p'} - M \ln \frac{p'_c}{p'} = 0 \quad (1)$$

where f is the yield function, q is the generalized shear stress, p' is the effective mean principal stress, p'_c is the effective pre-consolidation pressure, M is the failure stress ratio.

Burland used the incremental plastic energy equation to modify the Cam-Clay model:

$$dW^p = p' \sqrt{(d\varepsilon_v^p)^2 + (d\varepsilon_s^p)^2} \quad (2)$$

where W^p is the plastic energy, ε_v^p is the plastic bulk strain, ε_s^e is the elastic bulk strain.

Therefore, the modified Cam-Clay model is derived as:

$$\left(p' - \frac{p'_c}{2} \right) + \left(\frac{q}{M} \right)^2 = \left(\frac{p'_c}{2} \right)^2 \quad (3)$$

It can be seen that the yield surface is an ellipse on the p' - q plane, and the top point is in the line that is expressed by $q=Mp'$ as shown in Figure 1.

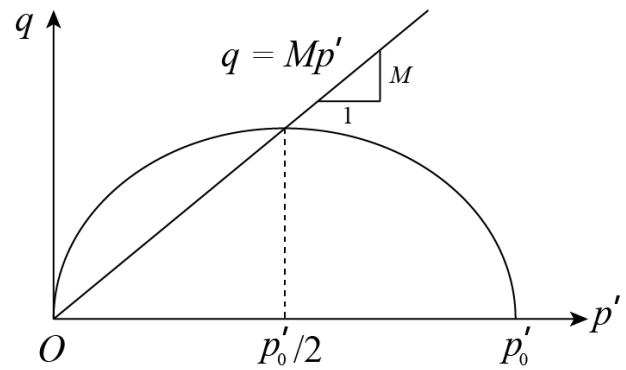


Fig. 1 The yield surface of the modified Cam-Clay model on the p' - q plane

Plasticity of the model

In the Cartesian coordinate system, the effective mean principal stress and the generalized shear stress can be expressed as:

$$\begin{cases} p' = \frac{1}{3}(\sigma'_x + \sigma'_y + \sigma'_z) \\ q = \left[\begin{aligned} &\sigma_x'^2 + \sigma_y'^2 + \sigma_z'^2 + 3(\tau_{xy}^2 + \tau_{yz}^2 + \tau_{zx}^2) \\ &-(\sigma'_x\sigma'_y + \sigma'_y\sigma'_z + \sigma'_z\sigma'_x) \end{aligned} \right]^{1/2} \end{cases} \quad (4)$$

where σ'_x , σ'_y , and σ'_z are normal stresses, τ_{xy} , τ_{yz} , and τ_{zx} are shear stresses.

The elastic bulk modulus of the modified Cam-Clay model K is stress-dependent, it can be calculated using the Equation (5).

$$K = \frac{1+e}{\kappa} p' \quad (5)$$

where e is the void ratio, κ is the slope of the rebound curve.

Hence, the three-dimensional elastic stiffness matrix with the assumption of isotropic material is:

$$\frac{3K(1-\mu)}{1+\mu} \begin{bmatrix} 1 & \frac{\mu}{1-\mu} & \frac{\mu}{1-\mu} & 0 & 0 & 0 \\ \frac{\mu}{1-\mu} & 1 & \frac{\mu}{1-\mu} & 0 & 0 & 0 \\ \frac{\mu}{1-\mu} & \frac{\mu}{1-\mu} & 1 & 0 & 0 & 0 \\ 0 & 0 & 0 & \frac{1-2\mu}{2(1-\mu)} & 0 & 0 \\ 0 & 0 & 0 & 0 & \frac{1-2\mu}{2(1-\mu)} & 0 \\ 0 & 0 & 0 & 0 & 0 & \frac{1-2\mu}{2(1-\mu)} \end{bmatrix}$$

(6)

where the μ is the poisson's ratio.

In the associated flow criterion, the flow vector is the partial derivative of the yield function with respect to the stress vector. Therefore, according to the Equations (3) and (4), the flow vector can be derived.

$$\mathbf{r} = \begin{bmatrix} \left(\frac{2}{9} + \frac{2}{M^2}\right)\sigma'_x + \left(\frac{2}{9} - \frac{1}{M^2}\right)(\sigma'_y + \sigma'_z) - \frac{1}{3}p'_c \\ \left(\frac{2}{9} + \frac{2}{M^2}\right)\sigma'_y + \left(\frac{2}{9} - \frac{1}{M^2}\right)(\sigma'_x + \sigma'_z) - \frac{1}{3}p'_c \\ \left(\frac{2}{9} + \frac{2}{M^2}\right)\sigma'_z + \left(\frac{2}{9} - \frac{1}{M^2}\right)(\sigma'_x + \sigma'_y) - \frac{1}{3}p'_c \\ \frac{6\tau_{xy}}{M^2} \\ \frac{6\tau_{yz}}{M^2} \\ \frac{6\tau_{zx}}{M^2} \end{bmatrix} \quad (7)$$

where \mathbf{r} is the flow vector.

And the equivalent plastic hardening modulus of the modified Cam-Clay model is:

$$A = \frac{1+e}{\lambda - \kappa} p'_c (2p' - p'_c) \quad (8)$$

where A is the plastic hardening modulus, λ is the slope of the compression curve.

Closest Point Projection Method

The closest point project method is a stable and effective method during the integration of elastoplastic stress [25]. Its main algorithms are the elastic prediction, plastic modification, and backward Euler implicit integration. For a time increment $\Delta t (t_n \rightarrow t_{n+1})$, the stress vector $\boldsymbol{\sigma}_n$, the yield stress p'_c , the void ratio e_n , and the strain increment $\Delta \boldsymbol{\varepsilon}$ are known, and the integration process is:

(1) Elastic prediction

The stress is considered as elastic in this step, so the elastic trial stress vector is:

$$\boldsymbol{\sigma}'^{tr} = \boldsymbol{\sigma}'_n + \mathbf{D}^e \Delta \boldsymbol{\varepsilon} \quad (9)$$

Where $\boldsymbol{\sigma}'^{tr}$ is the effective elastic trial stress vector, $\boldsymbol{\sigma}'_n$ is the effective stress vector, \mathbf{D}^e is the elastic stiffness matrix as expressed by Equation (6).

Assume that the bulk modulus \bar{K} can get better results, then:

$$p'_{n+1} = p'_n + \Delta p' = p'_n + \bar{K} \Delta \varepsilon_v \quad (10)$$

When the time increment is small, Equation (11) can be derived.

$$p'_{n+1} = p'_n \exp\left(\frac{1+e_n}{\kappa} \Delta \varepsilon_v\right) \quad (11)$$

Therefore, Equation (12) can be get with the combination of Equations (10) and (11).

$$\bar{K} = \frac{p'_n}{\Delta \varepsilon_v} \left[\exp\left(\frac{1+e_n}{\kappa} \Delta \varepsilon_v\right) - 1 \right] \quad (12)$$

(2) Judgment of yielding

According to the elastic trial stress vector, the trial stresses can be calculated, and the value of the yield function also can be calculated: if the value is not greater than 0, the elastic status is kept, then the integration of stress is finished; otherwise, the integration of elastoplastic stress should be executed in the next step.

(3) Integration of elastoplastic stress

In this step, the elastic trial stress would be iteratively improved. The iterations adopt the backward Euler implicit integration that does not need to solve the intersections between the stress path and the yield surface.

According to the theory of the modified Cam-Clay model, equations for the backward Euler implicit integration can be described as:

$$\begin{cases} \tilde{\sigma}'_{n+1} = \sigma'_n + \mathbf{D}^{n+\theta} \Delta \boldsymbol{\varepsilon} - \Lambda \mathbf{D}^{n+\theta} \mathbf{r}_{n+1} \\ \tilde{p}'_c{}^{n+1} = p'_c{}^n - \Lambda \frac{1+e}{\lambda-\kappa} p'_c{}^{n+1} (2p'_{n+1} - p'_c{}^{n+1}) \\ \tilde{f}_{n+1} = \frac{q_{n+1}^2}{M^2} + p'_{n+1} (2p'_{n+1} - p'_c{}^{n+1}) \end{cases} \quad (13)$$

Between two iterative steps, the bulk modulus is calculated using the θ method as expressed in Equation (14).

$$\begin{cases} \sigma'_{n+\theta} = (1-\theta)\sigma'_n + \theta\sigma'_{n+1} \\ K_{n+\theta} = \frac{1+e_n}{\kappa} p'_{n+\theta} \end{cases} \quad (14)$$

Therefore, the residuals of the integration equations are:

$$\begin{cases} \mathbf{R}_\sigma = \sigma'_{n+1} - [\sigma'_n + \mathbf{D}^{n+\theta} \Delta \boldsymbol{\varepsilon} - \Lambda \mathbf{D}^{n+\theta} \mathbf{r}_{n+1}] \\ R_c = p'_c{}^{n+1} - p'_c{}^n + \Lambda \frac{1+e}{\lambda-\kappa} p'_c{}^{n+1} (2p'_{n+1} - p'_c{}^{n+1}) \\ R_f = \frac{q_{n+1}^2}{M^2} + p'_{n+1} (p'_{n+1} - p'_c{}^{n+1}) \end{cases} \quad (15)$$

Where Λ is the plastic factor.

The residuals listed in Equation (15) should be eliminated to find the increments for the next iterative step. Finally, the system equations are:

$$\begin{cases} \mathbf{A} \delta \boldsymbol{\sigma}' + \mathbf{B} \delta p'_c + \mathbf{F} \delta \Lambda = -\mathbf{R}_\sigma \\ \mathbf{H}^T \delta \boldsymbol{\sigma}' + \omega \delta p'_c + \beta \delta \Lambda = -R_c \\ \mathbf{E}^T \delta \boldsymbol{\sigma}' + \gamma \delta p'_c = -R_f \end{cases} \quad (16)$$

Where $\delta \boldsymbol{\sigma}'$, $\delta p'_c$, $\delta \Lambda$ are the iterative corrections, \mathbf{A} , \mathbf{B} , \mathbf{F} , \mathbf{H} and \mathbf{E} are coefficient matrices, β , ω , γ are system coefficients.

The coefficients in equation (16) is the partial derivative of the residual value with respect to the correction variable. Solving equation (16) can get iterative corrections. After updating, it is judged whether the solving process has converged. If not, the integration of plastic stress should be repeated using the updated values until the convergence is reached. The criteria for iterative convergence can be as follows:

$$\begin{cases} err_\sigma = \|\mathbf{R}_\sigma^{k+1}\| / \|\boldsymbol{\sigma}_{n+1}^k\| \leq TOL_\sigma \\ err_c = R_c^{k+1} / p_c^{m+1,k} \leq TOL_c \\ err_f = R_f^{k+1} = f^{k+1} \leq TOL_f \end{cases} \quad (17)$$

Where err and TOL indicates relative errors and tolerance respectively, k is the number of iterations.

In order to make the iteration more efficient, the initial value of plastic factor Λ can be calculated by the following equation:

$$\Lambda = \frac{f^{tr}}{(\mathbf{r}^{tr})^T \mathbf{D}^e \mathbf{r}^{tr} + A^{tr}} \quad (18)$$

At the end of the plastic stress integration, the elastoplastic stiffness matrix of the elastoplastic incremental constitutive relationship needs to be calculated [26]:

$$\mathbf{D}^{ep} = \mathbf{D}^e - \frac{\mathbf{D}^e \mathbf{r} \mathbf{r}^T \mathbf{D}^e}{A + \mathbf{r}^T \mathbf{D}^e \mathbf{r}} \quad (19)$$

Implementation

Based on the detailed theory in previous sections, a material constitutive subroutine embedded in ABAQUS is developed using FORTRAN.

III. VERIFICATION

The triaxial compression test is commonly used to determine the calculation parameters of the soil and reveal the characteristics of the soil. The triaxial compression test is simulated in this section to

verify the feasibility, stability, and accuracy of the UMAT subroutine model in ABAQUS, at the same time the features of the modified Cam-Clay model is revealed.

Model paramters

Figure 2 shows a cube with a side length of 1m. The S1 surface is constrained in the X direction, the S2 surface is constrained in the Y direction, and the S3 surface is constrained in the Z direction. For the triaxial test with stability after pre-consolidated, the same confining pressure is applied on the S4, S5, and S6 surfaces. Hence, the initial stress state of the soil is confirmed, and the initial consolidation state of the soil can be determined. Subsequently, the confining pressure is unchanged, so that the surface forces on the S4 and S5 surfaces remain unchanged, and then the external pressure is applied on the S6 surface until the soil is broken.

In the calculation process, the compression process can be controlled by stress or displacement. Considering that the displacement control is more flexible, this simulation adopts the displacement control method. It means that the negative displacement is applied on the S6 surface in the Z direction, and the maximum axial strain reaches 40% in this test.

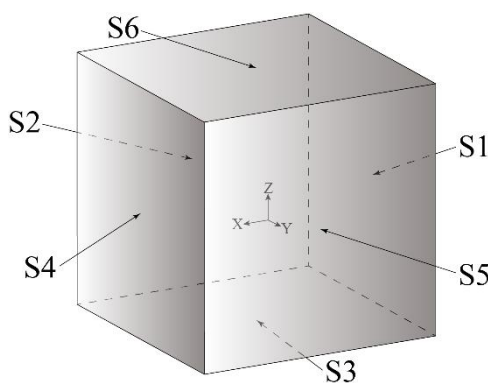


Fig. 2The model of the triaxial test

In this simulation, three initial consolidation states are considered: normal consolidation ($OCR=1$), weak overconsolidation ($OCR=2$) and heavy overconsolidation ($OCR=5$). The calculation parameters are listed in Table 1. In addition, only

the drainage consolidation case is considered for the verification.

Table 1 Calculation parameters of the triaxial test

	$OCR=1$	$OCR=2$	$OCR=5$
Initial confining pressure(kPa)	200	400	100
Initial yield stress(kPa)	200		
λ	0.066		
κ	0.0077		
M	1.2		
e_0	1.0		
μ	0.3		

Simulation of drainage consolidation

In the drainage consolidation test, the drainage is carried out during the compression process. It can be considered that the pore pressure is 0 during the compression process, that is, the effective stress is equal to the total stress. According to the Equation (4), it can be seen that the stress path of the drainage consolidation on the $p'-q$ plane is a straight line and the slope is $k=\Delta q/\Delta p'=3$.

For the case where the slope of the stress path k is constant, Dunja Perić [27] has derived the analytical solution of the strain under the drainage consolidation. Considering a time increment step $\Delta t(t_n \rightarrow t_{n+1})$, p' and q at t_n and t_{n+1} are known, and the void ratio e_n at the beginning of the increment step is given, the analytical solution of the elastic strain increment is:

$$\begin{cases} \Delta \varepsilon_v^e = \frac{1}{1+e_n} \ln \left(\frac{p'_{n+1}}{p'_n} \right)^{-\kappa} \\ \Delta \varepsilon_s^e = \frac{1}{1+e_n} \ln \left(\frac{k-\eta_{n+1}}{k-\eta_n} \right)^{-\frac{2k\kappa(1+\mu)}{9-18\mu}} \end{cases} \quad (20)$$

Where $\eta=q/p'$.

The plastic strain increment under the elastoplastic status is:

$$\left\{ \begin{aligned} \Delta \varepsilon_V^p &= \frac{1}{1+e_n} \ln \left[\left(\frac{p'_{n+1}}{p'_n} \right)^{-\lambda} \left(\frac{M^2 + \eta_{n+1}^2}{M^2 + \eta_n^2} \right)^{\kappa-\lambda} \right] \\ \Delta \varepsilon_S^p &= \frac{1}{1+e_n} \left\{ \ln \left[\left(\frac{M - \eta_{n+1}}{M - \eta_n} \right)^a \left(\frac{M + \eta_{n+1}}{M + \eta_n} \right)^b \left(\frac{k - \eta_{n+1}}{k - \eta_n} \right)^c \right] \right. \\ &\quad \left. - \frac{2(\lambda - \kappa)}{M(1+e_n)} \left[\arctan \left(\frac{\eta_{n+1}}{M} \right) - \arctan \left(\frac{\eta_n}{M} \right) \right] \right\} \\ a &= \frac{(\lambda - \kappa)k}{M(M - k)} \\ b &= \frac{(\lambda - \kappa)k}{M(M + k)} \\ c &= \frac{3(\lambda - \kappa)k}{k^2 - M^2} \end{aligned} \right. \quad (21)$$

At the end of the increment step, the increments of axial strain, radial strain, and void ratio are:

$$\left\{ \begin{aligned} \Delta \varepsilon_a &= \frac{1}{3} \Delta \varepsilon_V + \Delta \varepsilon_S \\ \Delta \varepsilon_r &= \frac{1}{3} \Delta \varepsilon_V - \frac{1}{2} \Delta \varepsilon_S \\ \Delta e &= -\frac{\Delta \varepsilon_V}{1+e_n} \end{aligned} \right. \quad (22)$$

Besides the analytical solution using DunjaPerić's equations, numerical calculations the ABAQUS built-in model and developed UMAT model in this research were carried out at the same time.

Results and discussions

According to the calculated results, the relationships of $\varepsilon_a - q$ and $\varepsilon_a - \varepsilon_V$ are shown in Figure 3, and the stress path in the $p'-q$ plane is shown in Figure 4.

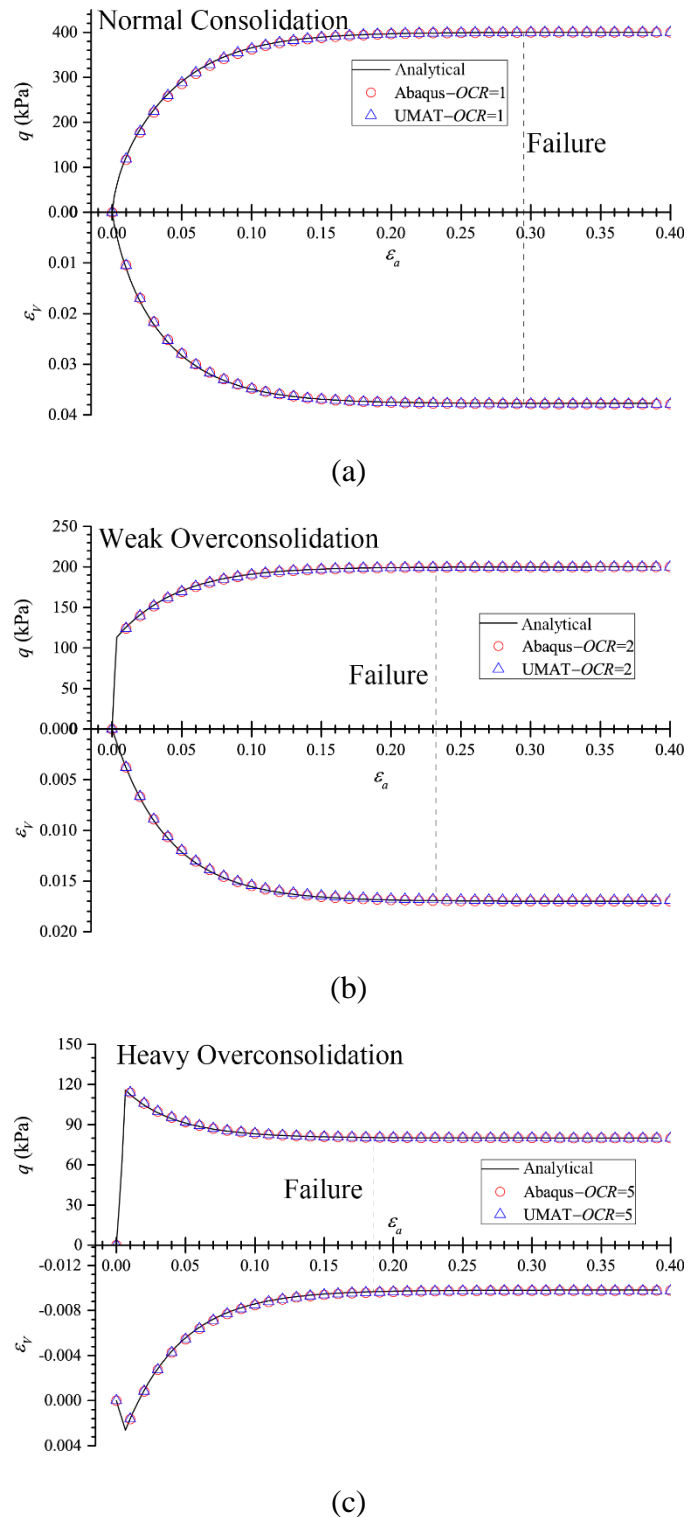


Fig. 3 $\varepsilon_a - q$ and $\varepsilon_a - \varepsilon_V$ curves of the triaxial compression drainage consolidation test

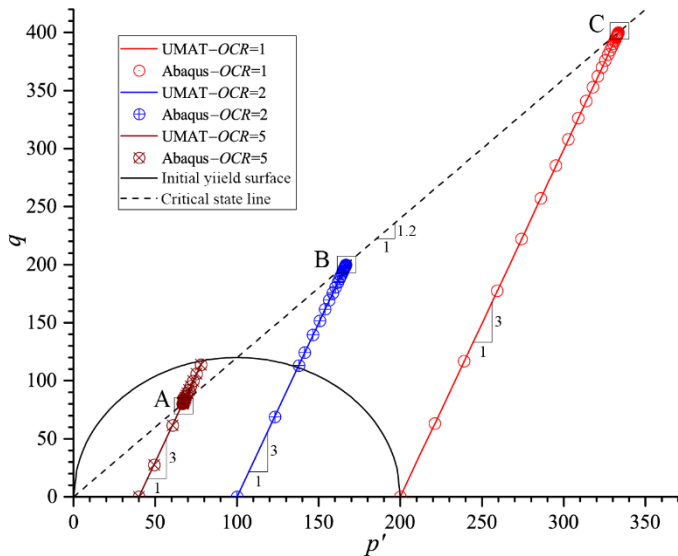


Fig. 4 p' - q curves of the triaxial compression drainage consolidation test

It can be seen from Figure 3 that the results calculated by the UMAT model are correct and stable. Results from the UMAT model, the ABAQUS built-in model, and the analytical equations are almost the same. At the same time, it can be seen that the relationship between the stress and the strain is linear when the soil is over-consolidated, whereas it is nonlinear when the soil is elastoplastic. From the (c) in Figure 3, the heavy overconsolidated soil exhibits an obvious softening phenomenon when it is elastoplastic, while it shows hardening law when it is normal consolidated or weak over-consolidated in (a) and (b). According to the $\varepsilon_a - \varepsilon_v$ curve in Figure 3, the volumetric strain increases during the elastic phase when it is triaxially compressed. However, when the soil is in the plastic phase, the volumetric strain of soils under normal consolidation or the weak overconsolidation increase (shear shrinkage), whereas it decreases when soils are under heavy overconsolidated soils and have a negative volumetric strain (shear dilatancy). In Figure 4, results illustrate that the stress path of drainage consolidation is a straight line with a slope of 3, the numerical calculation results are consistent with the theory.

It can be seen from Figure 4 that a lot of data points are gathered at three points A, B, and C. In fact, this means that the stresses after failure are on the critical state line on the p' - q surface. The stress status when the failure occurs can be obtained, as listed in Table 2. As Figure 3 shown, the shear stress q and volumetric strain ε_v after failure are unchanged, and at the same time, it can be seen that as the ratios of overconsolidation increase, the axial strain at failure in consolidation drainage decreases.

Table 2 Stress and strain at the initial failure of the triaxial compression drainage consolidation

	OCR=1	OCR=2	OCR=5
p' (kPa)	333.33	166.67	66.67
q (kPa)	400	200	80
ε_a (%)	29.4	23.2	18.6
ε_v (%)	3.77	1.70	-0.98

IV. CONCLUSION

The integration equations of the elastoplastic stress of the modified Cam-Clay model under the Cartesian coordinate space using the closest point projection method were derived in this paper, and the UMAT subroutine of this model in ABAQUS was developed using FORTRAN. Finally, the triaxial compression tests under drainage consolidation are conducted for verifications. From the calculated results, three main conclusions are summarized as follows:

- (1) The modified Cam-Clay model can describe the behaviors of the soft clay well. It is better to choose the modified Cam-Clay model for analyses of projects built-on soft ground.
- (2) The closest point projection method is a proper method for the integration of the elastoplastic stress in the modified Cam-Clay model. Numerical experiments show that it is feasible and stable.
- (3) All the equations derived in this paper are in the Cartesian coordinate system, therefore they fit real

three dimensional cases. Verification results indicate that the equations are accurate enough.

REFERENCES

- [1] Roscoe K.H. (1963) Mechanical behaviour of an idealized 'wet' clay. Proc. 3rd Eur. Conf. Soil Mech (1): 47-54.
- [2] Roscoe K.H. (1958) On The Yielding of Soils. Géotechnique (8): 22-53.
- [3] Roscoe K.H. and Burland J.B. (1968) On the Generalized Stress-Strain Behavior of Wet Clay. Engineering plasticity.
- [4] Kasper T. and Meschke G. (2004) A 3D finite element simulation model for TBM tunnelling in soft ground. International journal for numerical and analytical methods in geomechanics (28): 1441-1460.
- [5] Sheng D., Eigenbrod K.D. and Wriggers P. (2005) Finite element analysis of pile installation using large-slip frictional contact. Computers and geotechnics (32): 17-26.
- [6] Stankiewicz A. and Pamin J. (2006) Finite element analysis of fluid influence on instabilities in two-phase Cam-clay plasticity model. Computer Assisted Mechanics and Engineering Sciences, (13): 669-682.
- [7] Kung G.T.C., Ou C.Y. and Juang C.H. (2009) Modeling small-strain behavior of Taipei clays for finite element analysis of braced excavations. Computers and Geotechnics (36): 304-319.
- [8] Likitlersuang S., Surarak C., Wanatowski D., Oh E. and Balasubramaniam A. (2013) Finite element analysis of a deep excavation: A case study from the Bangkok MRT. Soils and foundations (53): 756-773.
- [9] Zhang W., Goh A.T. and Xuan F. (2015) A simple prediction model for wall deflection caused by braced excavation in clays. Computers and Geotechnics (63): 67-72.
- [10] Likitlersuang S., Teachavorasinskun S., Surarak C., Oh E. and Balasubramaniam A. (2013) Small strain stiffness and stiffness degradation curve of Bangkok Clays. Soils and Foundations (53): 498-509.
- [11] Kung G.T.C. (2009) Comparison of excavation-induced wall deflection using top-down and bottom-up construction methods in Taipei silty clay. Computers and Geotechnics (36): 373-385.
- [12] Dong Y.P., Burd H.J. and Houlsby G.T. (2016) Finite-element analysis of a deep excavation case history. Géotechnique (66): 1-15.
- [13] Callari C., Auricchio F. and Sacco E. (1998) A finite-strain Cam-clay model in the framework of multiplicative elasto-plasticity. International Journal of Plasticity (14): 1155-1187.
- [14] Sheng D., Sloan S. W., Gens A. and Smith D. W. (2003) Finite element formulation and algorithms for unsaturated soils. Part I: Theory. International journal for numerical and analytical methods in geomechanics (27): 745-765.
- [15] Hashash Y.M. and Whittle A.J. (1992) Integration of the modified Cam-clay model in non-linear finite element analysis. Computers and geotechnics (14): 59-83.
- [16] Yamakawa Y., Hashiguchi K. and Ikeda K. (2010) Implicit stress-update algorithm for isotropic Cam-clay model based on the subloading surface concept at finite strains. International Journal of Plasticity (26): 634-658.
- [17] Liu K., Chen S.L. and Voyiadjis G.Z. (2019) Integration of anisotropic modified Cam Clay model in finite element analysis: Formulation, validation, and application. Computers and Geotechnics (116): 103198.
- [18] Borja R.I. and Lee S.R. (1990) Cam-clay plasticity, part 1: implicit integration of elasto-plastic constitutive relations. Computer Methods in Applied Mechanics and Engineering (78): 49-72.
- [19] Borja R.I. (1991) Cam-Clay plasticity, Part II: Implicit integration of constitutive equation based on a nonlinear elastic stress predictor. Computer Methods in Applied Mechanics and Engineering (88): 225-240.
- [20] Borja R.I. and Tamagnini C. (1998) Cam-Clay plasticity Part III: Extension of the infinitesimal model to include finite strains. Computer Methods in Applied Mechanics and Engineering (155): 73-95.
- [21] Borja R.I., Tamagnini C. and Alarcón, E. (1998) Elastoplastic consolidation at finite strain part 2: finite element implementation and numerical examples. Computer Methods in

- Applied Mechanics and Engineering (159): 103-122.
- [22] Yao Y.P. and Sun D.A. (2000) Application of Lade's criterion to Cam-clay model. *Journal of engineering mechanics* (126): 112-119.
- [23] Ortiz M, Pandolfi A. (2004) A variational Cam-clay theory of plasticity. *Computer Methods in Applied Mechanics and Engineering* (193): 2645–2666.
- [24] Krabbenhoft K., Lyamin A.V. (2012) Computational Cam clay plasticity using second-order cone programming. *Computer Methods in Applied Mechanics and Engineering* (209): 239–249.
- [25] Anandarajah A. (2011) *Computational Methods in Elasticity and Plasticity: Solids and Porous Media*. Springer Science & Business Media.
- [26] Duncan J.M., Chang C.Y. (1970) Nonlinear analysis of stress and strain in soils. *Journal of the Soil Mechanics and Foundations Division, ASCE* (96): 1629–1653.
- [27] PERIĆ D. (2006) Analytical solutions for a three-invariant Cam clay model subjected to drained loading histories. *International Journal for Numerical and Analytical Methods in Geomechanics* (30): 363–387.